Atmósfera (1993), 6, pp. 51 - 77

Studies of CISK

A. WIIN-NIELSEN

Geophysical Institute, University of Copenhagen, Haraldsgade 6, 2200 Copenhagen N, Denmark

(Mansucript received Feb. 18, 1992; accepted in final form June 26, 1992

RESUMEN

La inestabilidad condicional de segunda clase (CISK) se somete a la investigación. Se emplea un modelo cuasi-geostrófico con una estabilidad estática variable en el sentido vertical para resolver exactamente el problema CISK. Debido a la naturaleza de la solución, ésta no puede ser calculada con ninguna precisión para longitudes de onda pequeña. Empleando funciones de estructura vertical no aparece ningún problema numérico excepto en las longitudes de onda muy pequeñas. La solución aproximada guarda un excelente acuerdo con la solución exacta, cuando ambas pueden ser evaluadas con buena precisión. La frecuencia puede obtenerse sumando una serie sin resolver el problema complejo.

El caso cuasi-geostrófico se generaliza al caso de las ecuaciones primitivas con unas pocas componentes verticales. La existencia de modos de gravedad inerciales tiene una influencia sobre la estabilidad del modo cuasi-geostrófico. Las ondas largas se vuelven más estables, pero para las cortas la diferencia entre los dos modos se torna muy pequeña, y en el límite donde la longitud de onda se anula, ambas se acercan a la solución llamada 'free-ride'. Se encuentran para las ondas cortas grandes desviaciones que difieren de la solución cuasi-geostrófica, como determinada, por ejemplo, por la razón de la divergencia a la vorticidad.

Un resultado final es que empleando las ecuaciones primitivas es importante expresar la velocidad vertical de razonamiento en términos de la función de corriente, pero no en función del geopotencial. El último procedimiento conduciría a modos espurios debido a un uso incongruente de las ecuaciones cuasi-geostróficas. Estos modos tienen un tiempo de doblaje en que es una fracción pequeña de una día.

ABSTRACT

The conditional instability of the second kind (CISK) is investigated. A quasi-geostrophic model with a variable static stability in the vertical direction is used to solve the CISK problem exactly. Due to the nature of the solution it cannot be calculated with any accuracy for small wavelenghts. Using vertical structure functions no numerical problems appear except for very small wavelenghts. The approximate solutions are in excellent agreement with the exact solution, when both of them can be evaluated with good accuracy. The frequency may be obtained by summing a series without solving the complete problem.

The quasi-geostrophic case is generalized to the case of the primitive equations with a few vertical components. The existence of the gravity-inertia modes has an influence on the stability of the quasi-geostrophic mode. The long waves become more stable, but for short waves the difference between the two modes become very small, and in the limit where the wavelength goes to zero both of them will approach the so-called 'free-ride' solution. Large deviations from the quasi-geostrophic solution, as measured for example by the ratio of divergence to vorticity, are found for the short waves.

A final result is that in using the primitive equations it is important to express the frictional vertical velocity in terms of the streamfunction, but not in terms of the geopotential. The latter procedure will lead to spurious modes due to an inconsistent use of the quasi-geostrophic equations. These spurious models have an e-doubling time which is a small fraction of a day.

1. Introduction

The CISK mechanism has been investigated extensively since it was first introduced by Charney and Eliassen (1964) and Ooyama (1964) in an attempt to describe the formation of a hurricane with its characteristic structure. CISK has also at a later time been proposed as a possible mechanism for the initiation and development of the polar lows (Rasmussen, 1979). Recently, Fräedrich and McBride (1989) have formulated a special version of the CISK-mechanism called the 'free ride'. In this formulation the vertical velocity is made directly proportional to the heating by neglecting local and advective changes in the thermodynamic equation. Pedersen (1991), hereafter referred to as SP, has compared the CISK procedure in the quasi-geostrophic case with a constant value of the static stability with the free ride. The two procedures agree with each other in the limit of very small wavelengths, but with rather large differences between the two solutions, as one would expect, for the larger scales.

The CISK-mechanism is of general interest because it shows the impact of the heat of condensation on the temperature and velocity fields. In agreement with SP we shall assume that all the moisture entering a vertical column through the top of the boundary layer is condensed, and that a distribution function describes the vertical distribution of the heating.

SP investigated a quasi-geostrophic model with a continuous vertical variation of the variables, but considered only the case of a constant static stability. Several earlier investigations employed a few vertical levels. We shall generalize the model by SP to a vertical stability which varies in the vertical direction as inversely proportional to the square of the pressure. We expect to find a different vertical variation of the dependent variables and a change in the stability of the mechanism. While both of the models can be solved exactly, it turns out that the solution in both cases is difficult to calculate for small wavelength due to the appearance of either power or exponential functions with very large values. A different formulation based on vertical structure functions (Kasahara and Tanaka, 1989; Wiin-Nielsen and Marshall, 1989, 1990) can be used. In that case the evaluations are possible with good accuracy, but as one would expect a large number of structure functions are needed. In particular, the evaluation of the stability creates no problems.

The application of quasi-geostrophic theory to small scales is difficult to justify. We shall attempt to extend the theory to the case of the primitive equations, but shall continue to consider perturbations on a basic state of rest in which case we may hope to maintain the basic assumption that the heating due to condensation will occur in the same vertical column into which the moisture was introduced.

Using the primitive equations we shall investigate the influence of the gravity-inertia modes on the quasi-geostrophic modes. A general solution using a large number of structure functions has not been accomplished, and we have restricted the case to the two-level model. In this case the eigenvalue problem leads to a simple algebraic equation, which may be solved numerically. However, if we are satisfied with the determination of the single mode, corresponding to the quasi-geostrophic mode, we may obtain this particular eigenvalue within the real domain.

2. Variable static stability

A variation of the static stability in the vertical direction is permissible in quasi-geostrophic models. Christensen and Wiin-Nielsen (1991) using global temperature data have shown that a good approximation is of the form

$$\sigma = \sigma_o \frac{p_o^\delta}{p^\delta} \tag{2.1}$$

where δ is an empirically determined constant. The value of the constant depends on how far into the stratosphere we have data, but a value close to $\delta = 2$ is representative for the troposphere and the lower stratosphere.

Adopting the same formulation as SP we find the omega equation:

$$\frac{f_o^2}{p_o^2}\frac{\partial^2\omega}{\partial p^2} + \sigma\nabla^2\omega = \sigma\nabla^2\omega_B\eta(p) \tag{2.2}$$

where the only difference is that the static stability is a function of pressure. In (2.2) we have introduced the nondimensional parameter $p = p_*/p_o$ where p_* is the pressure and $p_o = 100$ kPa is a standard value for the surface pressure. f_o is the constant value of the Coriolis parameter, and $\eta = \eta(p)$ is the heating distribution function. We seek solutions of (2.2) of the form:

$$\omega = \hat{\omega}(p)e^{\nu t}\cos(kx) \tag{2.3}$$

where ν is the growth rate and $k = 2\pi/L$ is the wave number and L the wavelength. After rearrangement we get

$$\frac{d^2\hat{\omega}}{dp^2} - \frac{\lambda^2}{p^2}\hat{\omega} = -\frac{\lambda^2}{p^2}\hat{\omega}_B\eta(p) \tag{2.4}$$

where

$$\lambda^2 = k^2/q^2,\ q^2 = f_o^2/(\sigma_o p_o^2)$$

Equation (2.4) will be solved with the boundary condition $\omega = 0$ for $p = p_T$, where p_T is different from zero. The reason is that the specification of the static stability prevents us from using the same condition at $p = 0$. At the lower boundary we have a choice. We can either apply the boundary condition at $p = p_B$, where p_B is the pressure at the top of the boundary layer, or we can apply the condition at $p = 1$. In the first case we have $\omega = \omega_B$ at $p = p_B$ while the second case gives $\omega = 0$ at $p = 1$. The choice comes from the fact that ω_B is a notation for the net effect of the frictional processes in the planetary boundary layer since ω_B is defined as the vertical velocity due to the stress at the surface under the assumption that there is a balance between the divergence term and the frictional terms in the boundary layer expressed as:

$$\omega_B = -\frac{g}{f_o}k_F\zeta_o = \frac{g}{f_o^2}k_F k^2\Phi_o \tag{2.5}$$

where k_F is the frictional coefficient.

To determine the frequency ν we use the vorticity equation

$$\frac{\partial\nabla^2\Phi}{\partial t} = \frac{f_o^2}{p_o}\omega_B\frac{d}{dp}\left(\frac{\omega}{\omega_B}\right) \tag{2.6}$$

Using (2.3) and (2.5) and applied at the lower boundary we get:

$$\nu = -\epsilon\frac{d}{dp}\left(\frac{\hat{\omega}}{\hat{\omega}_B}\right)_1 \tag{2.7}$$

in which

$$\epsilon = \frac{g}{p_o} k_F = 2.2 \times 10^{-6} s^{-1} \tag{2.8}$$

After this discussion of the boundary condition we return to (2.4) which may be expressed in the variable ω/ω_B and solved by standard methods. The solutions to the homogeneous equation are power functions in p where the exponents satisfy the condition

$$\epsilon_1 + \epsilon_2 = 1; \quad \epsilon_1 = 1/2(1 + (1 + 4\lambda^2)^{1/2}) \tag{2.9}$$

while a solution to the inhomogeneous equation is:

$$\left(\frac{\omega}{\omega_B}\right) = p^{\epsilon_2} \int_1^p \frac{\lambda^2 \eta(p) p^{\epsilon_1 - 2}}{\epsilon_1 - \epsilon_2} dp - p^{\epsilon_1} \int_1^p \frac{\lambda^2 \eta(p) p^{\epsilon_2 - 2}}{\epsilon_1 - \epsilon_2} dp \tag{2.10}$$

The integrals in (2.10) are to be evaluated knowing the heat distribution function which is specified in advance. Finally, the two integration constants are determined from the boundary conditions.

We note finally that the integral condition on the distribution function (see SP) in this case turns out to be:

$$\int_{p_T}^1 \frac{\eta(p)}{p} dp = E_o \tag{2.11}$$

The numerical value of E_o can be obtained by noting that the transport of mass through the lower boundary of a column is $\rho_w W_B$ where ρ_w is the density of water vapor and W_B is the vertical velocity at the top of the boundary layer. Introducing the mixing ratio $q = \rho_w/\rho$ and converting the vertical velocity in the p-system we get

$$\rho_w W_b = \frac{q}{g} \omega_B \tag{2.12}$$

Assuming that all the moisture entering the column is condensed we find that the heating is:

$$H = -L \frac{q}{g} \omega_B \frac{g}{\Delta p} \tag{2.13}$$

where L is the heat of condensation, and where we have calculated the heating per unit mass. With the formulation used in this study we have:

$$-\frac{R}{C_p} \frac{1}{p} H = \frac{\sigma_o p_o}{p^2} \omega_B \eta(p) \tag{2.14}$$

Substituting from (2.13) in (2.14) we find that:

$$\int_{p_T}^1 \frac{\eta(p)}{p} dp = \frac{R}{C_p} \frac{Lq}{\sigma_o p_o \Delta p} \cong 2.8 \tag{2.15}$$

In calculating the value we have used:

$$L = 2.5 \times 10^6 kJt^{-1}, \quad q = 3 \times 10^{-2}, \quad \sigma_o = 0.85, \quad p_o = 100kPa, \quad \Delta p = 90kPa$$

The general procedure is then to specify $\eta(p)$, integrate (2.10), find the two integration constants depending on the selected boundary conditions and thereby obtain the solution for the scaled vertical velocity. Finally, the growth rate is determined from (2.7).

The solution obtained in this way suffers from some numerical difficulties which can be traced to the fact that it contains the two power functions entering the solutions to the homogeneous equation. ϵ_1 depends on λ^2 only, but this quantity is:

$$\lambda^2 = \frac{k^2}{q^2} \cong \frac{4\pi^2}{l^2} \tag{2.16}$$

where l is the wavelength measured in thousands of km. In our problem we are interested in small wavelenghts. Suppose for example that $L = 10$ km, i.e. $1 = 0.01$. We find $\lambda^2 = 4 \times 10^5$. This value corresponds to a value of $\epsilon_1 = 317$, and since the solution depends on powerfunctions with exponents of this order of magnitude it is obvious that it is impossible to obtain the required accuracy for small values of the non-dimensional pressure. It will thus be impossible to obtain the limiting value by numerical means when the wavelength goes to zero. On the other hand this limiting value can be obtain from (2.2) when $k \to \infty$ in which case we obtain:

$$\frac{\omega}{\omega_B} = \eta(p), \quad k \to \infty \tag{2.17}$$

and thus

$$\nu = -\epsilon \left(\frac{d\eta}{dp}\right)_1, \quad k \to \infty \tag{2.18}$$

which is the so-called free ride solution as shown by SP, but originally introduced by Fräedrich and McBride (1989).

In view of the numerical difficulties described above it is desirable to seek a solution to the CISK problem in a different form. For this problem we turn to the use of vertical structure functions as used by Kasahara and Tanaka (1989) and Wiin-Nielsen and Marshall (1990). It is then more convenient to work with the potential vorticity equation than with the omega equation because the structure functions for the geopotential form a normalized, orthogonal set. The quasi-geostrophic, potential vorticity equation is in our case as follows:

$$\frac{\partial}{\partial t}\left[\nabla^2\Phi + \frac{\partial}{\partial p}\left(\frac{f_o^2}{\sigma p_o^2}\frac{\partial \Phi}{\partial p}\right)\right] = -\epsilon \nabla^2 \Phi_o \frac{d\eta}{dp} \tag{2.19}$$

expressing that it is the vertical variation of the heating which changes the potential vorticity.

For a given heating distribution fuction $\eta = \eta(p)$ and for $\sigma = \sigma(p)$ obeying (2.1) with $\delta = 2$ we develop the geopotential in series of the form:

$$\phi = \sum_{n=1}^{\infty} \Phi(n) G_n(p) \tag{2.20}$$

where $G_n(p)$ are the structure functions as defined by Wiin-Nielsen and Marshall (1990) to

which the reader is referred for details. It suffices to say that these functions form a normalized, orthogonal set. We note further that

$$\phi_o = \sum_{n=1}^{\infty} \Phi(n) G_n(1) \tag{2.21}$$

and we define finally the coefficients $h(n)$ in such a way that

$$\frac{d\eta}{dp} = \sum_{n=1}^{\infty} h(n) G_n(p) \tag{2.22}$$

The coefficients $h(n)$ may thus be computed from the given distribution function. Assuming as before that the format (2.3) applies to the geopotential as well we obtain from the basic equation for the rate of change of the potential vorticity the following infinite set of equations:

$$\nu \Phi(n) + r(n) h(n) \sum_{s=1}^{\infty} \Phi(s) G_s(1) = 0 \tag{2.23}$$

(2.23) represents a standard eigenvalue problem which could be solved by suitable numerical procedures. However, in this case the equations are structured in such a way that ν can be determined directly. $r(n)$ in (2.23) is defined by:

$$r(n) = \epsilon \frac{k^2}{k^2 + q^2 \lambda(n)^2} \tag{2.24}$$

We proceed as follows. All variables except $\Phi(1)$ and $\Phi(2)$ are eliminated from the first two equations. We find that

$$\Phi(1) = \frac{r(1)h(1)}{r(2)h(2)} \Phi(2) \tag{2.25}$$

A similar procedure is used for each of the following pairs of equations with analogous results. Combining all the equations anologous to (2.25) we find as a general result:

$$\Phi(i) = \frac{r(i)h(i)}{r(N)h(N)} \Phi(N) \tag{2.26}$$

where N is the total number of variables. Inserting (2.26) in the last equation ($n = N$) of (2.23) we find that

$$\nu = - \sum_{n=1}^{N} r(n) h(n) G_n(1) \tag{2.27}$$

This finishes the formal development of the method of solution. The vertical structure functions were introduced in this study to avoid the numerical differences for small values of the wave-length. It should be pointed out that a rather large number of structure functions are needed to obtain good accuracy as one would expect in regions of compensating effects.

3. Some examples

The chosen example selects a flexible heating distribution which can be used to investigate its importance for the stability connected with the CISK mechanism. For this purpose we consider the following specification:

$$\eta(p) = \eta_m \frac{p(1-p)(p-p_T)}{N_o^2}(C_1 p + C_2) \tag{3.1}$$

where

$$N_o = p_m(1-p_m)(p_m - p_T) \tag{3.2}$$

and where C_1 and C_2 have been computed in such a way that $\eta(p)$ has an extremum η_m at $p = p_m$.

We find

$$C_1 = 3p_m^2 - 2(1+p_T)p_m + p_T \tag{3.3}$$

$$C_2 = p_m[4p_m^2 - 3(1+p_T)p_m + 2p_T] \tag{3.4}$$

The value of η_m is then for each value of p_m calculated from (2.11). The first calculation is carried out for $p_T = 0.05$ and $p_m = 0.8$. Figure 1 shows the e-folding time for the exact solution obtained from (2.4). It is seen that it approaches the special value for $L = 0$ which is obtained separately. The e-folding time can be computed with good accuracy because it depends only on values at $p = 1$. For the same case the e-folding time is also calculated using the structure functions for $N = 100$. For all practical purposes the values fall on the curve for small values of L, but small deviations can be observed for larger values of L as seen from the two marks on Figure 1 for $L = 2000$ km and $L = 2500$ km. The difference is however, in no case larger than 1.5%. Figure 2 shows how the e-folding time depends on the maximum number of structure functions for $L = 100$ km. It appears that the e-folding time has obtained its correct value for $N = 50$, but large deviations are observed for $N < 10$. Numerical values obtained for small values of N may thus have the correct sign, but may be off by an order of magnitude in the size of the e-folding time.

The distribution function for the present case is shown in Figure 3. It has a maximum heating in the lower part of the atmosphere and weak cooling in the upper part of the atmosphere. The latter may simulate processes above the cloud tops such as radiative cooling. The stability is strongly dependent on the shape of the distribution function. Figure 4 shows that if the maximum occurs in the higher part of the atmosphere one obtains stability for all wavelengths. For a slightly lower position of the maximum we find stability for the short waves as seen in Figure 5. A still lower maximum, Figure 6, shows instability for all wavelengths, but a maximum instability for $L = 500$ km. Figure 7 has its maximum at such a low level that the figure becomes similar to Figure 1. Figure 8 corresponds to a maximum at $p_m = 0.9$, but also a maximum close to $p = 0.45$ which is the value used for Figure 5. It is therefore not surprising that the stability diagrams have the same structure. Some care has to be used in the application of the distribution function given in (3.1) because it results in an extremum value, but the sign of η_m will show if we are at a maximum or a minimum. The relative vertical velocity, normalized by ω_B, and the relative geopotential, normalized by the value at $p = 1$, are displayed in Figure 9 for $L = 100$ km. For such a small value of the wavelength one finds a distribution of the vertical velocity very

similar to the distribution function for the heating. The geopotential, shown in the lower part of the figure, is consistent with the vertical velocity as can be seen from the relation between these two parameters in the present model. It is:

$$-\nu k^2 \Phi = \frac{f_o^2}{p_o} \frac{d\omega}{dp} \tag{3.5}$$

This equation shows that the sign of the geopotential is determined by the derivative of the vertical velocity and of the sign of the frequency. Figure 9 which presents a case of instability has $\Phi > 0$ where $d\omega/dp < 0$. In the opposite case of stability we will have $\Phi > 0$ whenever $d\omega/dp > 0$ as shown in Figure 10, where the maximum is located in the upper part of the atmosphere, and where we have selected a small wavelength of 100 km. Instability occurs in the same case for longer waves. Figure 11 shows an example for $L = 1500$ km.

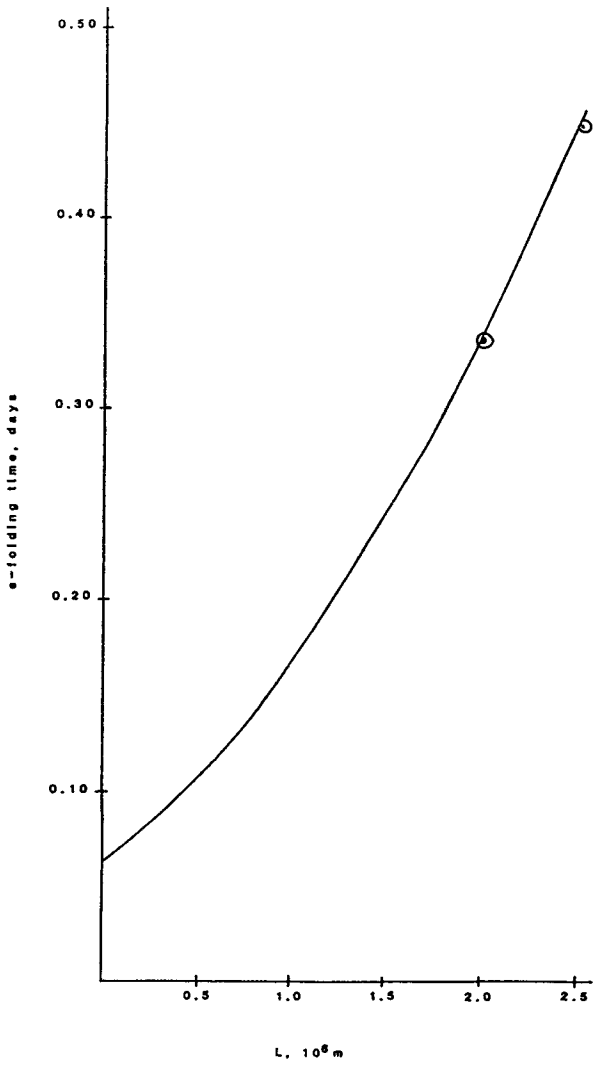

Fig. 1. The curve shows the e-folding time as a function of wavelength computed from the exact solution with $p_T = 0.05$ and $p_m = 0.8$ and $\eta_m = 7.0103$. The e-folding times are also calculated using structure functions. The two dots for $L = 2000$ km and $L = 2500$ km shows the accuracy.

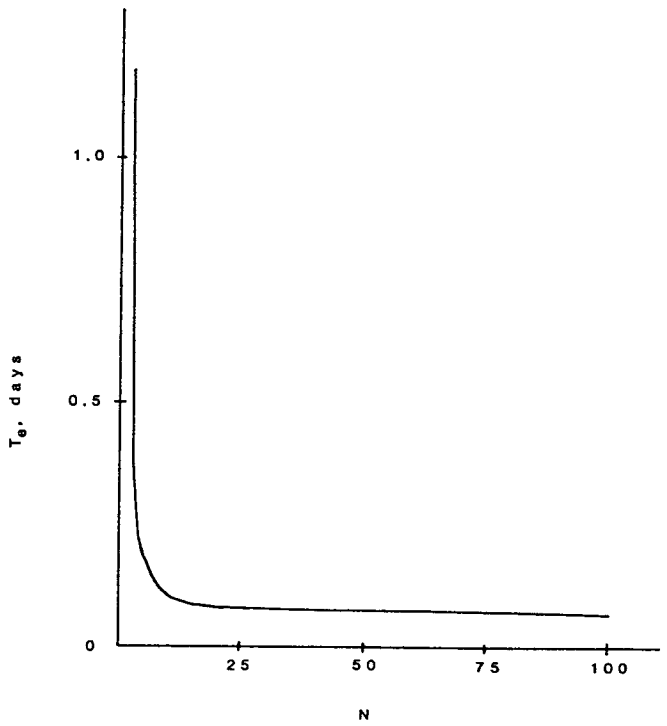

Fig. 2. The e-folding time as a function of the number of structure functions. Same parameters as in Fig. 1, but $L = 100$ km.

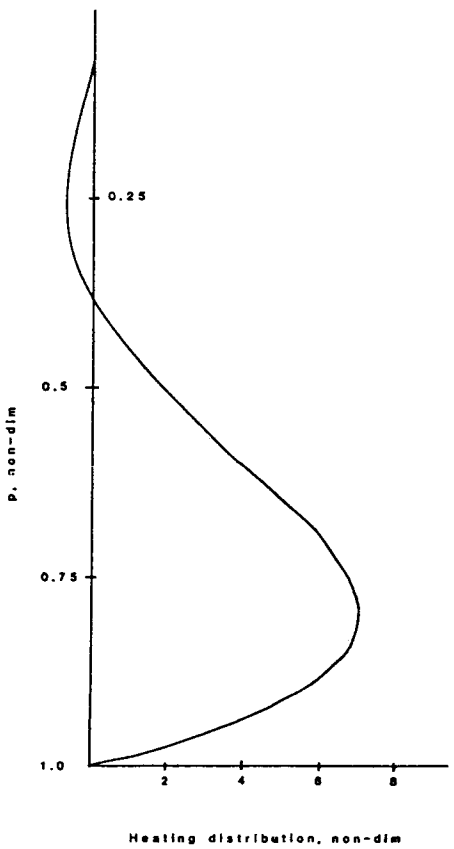

Fig. 3. The heating distribution function used in Fig. 1 and Fig. 2.

The cases described above were computed using the structure functions with $N = 100$. Otherwise it would not have been possible to calculate the solutions for small values of the wavelength. A comparison was also made with the case of constant static stability as used in SP. This case displays the same numerical difficulties for the smaller scales, and it is also in this case an advantage to use structure functions. They are simple trigonometric functions in the case of constant σ. Some comparative cases were computed with the result that the simpler case gives qualitatively correct results for the stability, but rather large differences in the vertical distributions of the parameters as one would expect.

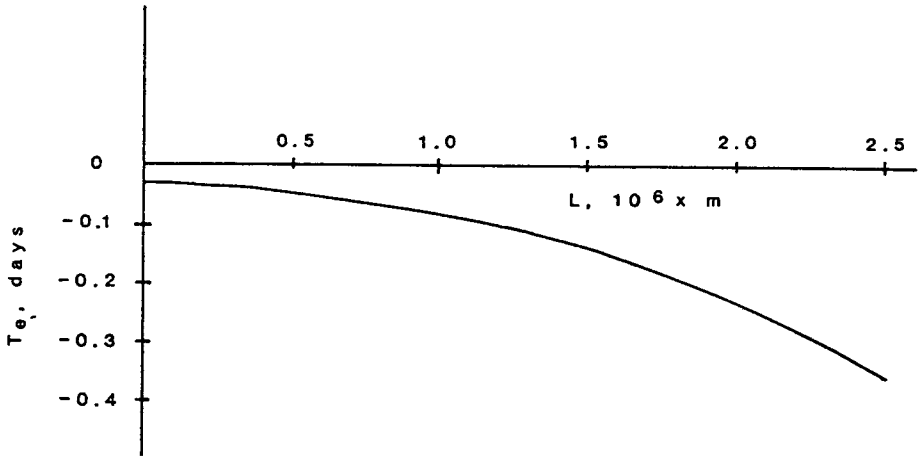

Fig. 4. The e-folding times shows stability for all wavelengths for $p_m = 0.35$ and $\eta_m = 7.1940$.

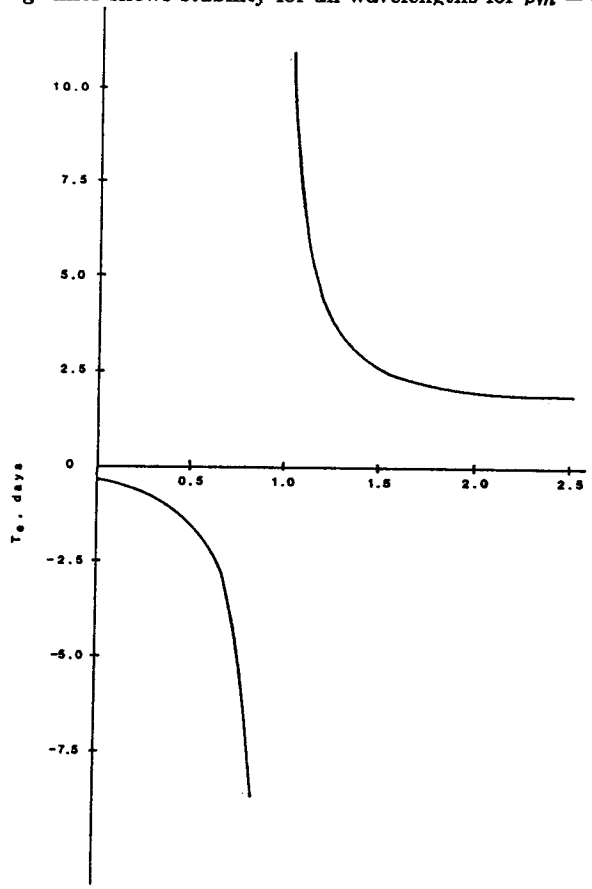

Fig. 5. For $p_m = 0.45$ and $\eta_m = 2.48$ one finds stability for the short waves and instability for the long waves.

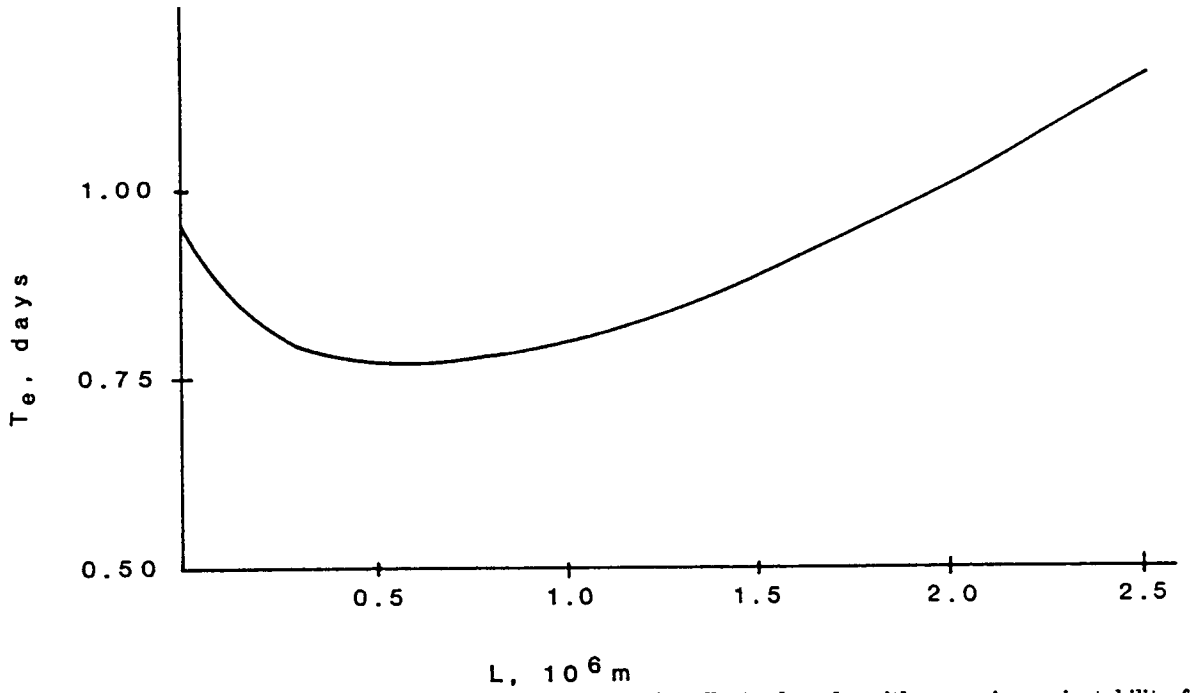

Fig. 6. For $p_m = 0.55$ and $\eta_m = 2.3318$ one finds instability for all wavelengths with a maximum instability for $L = 500$ km.

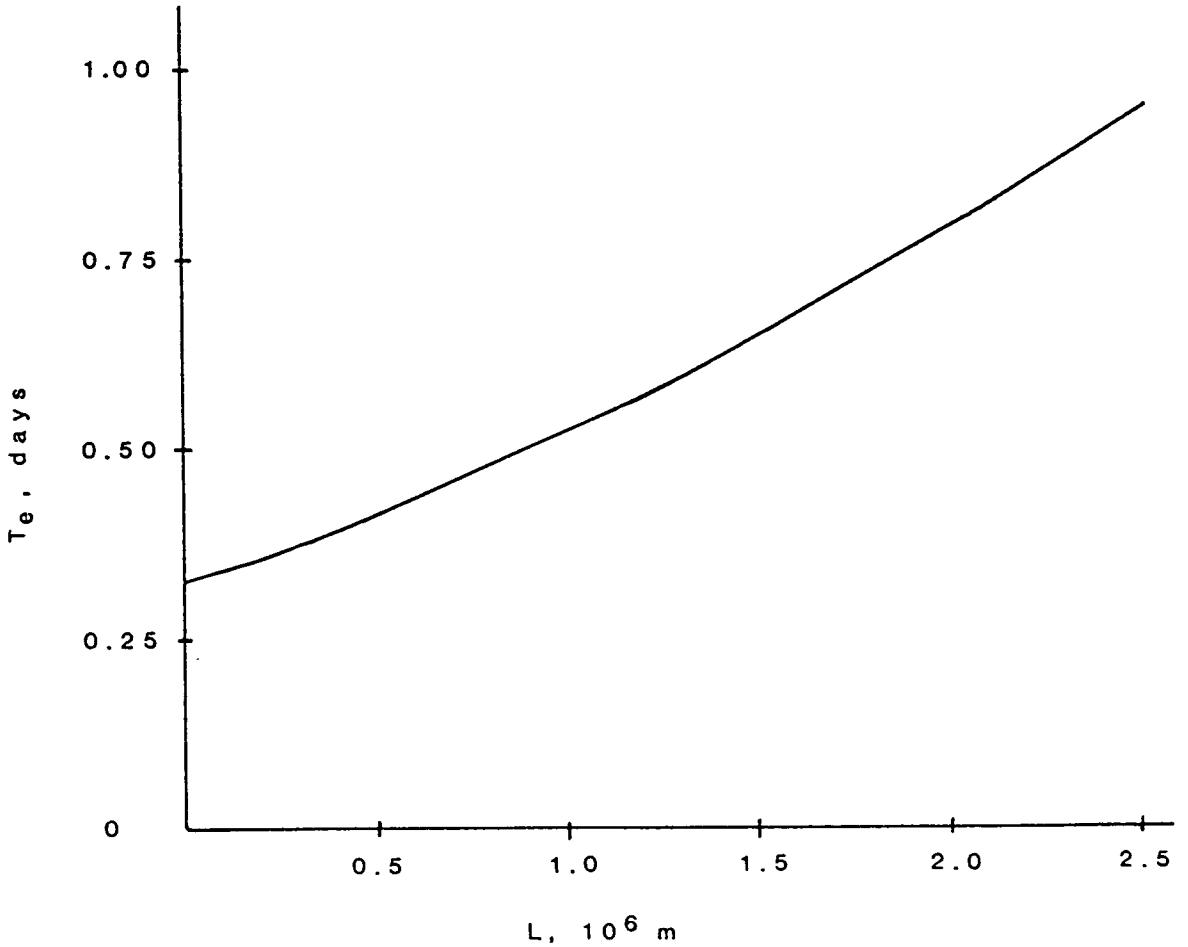

Fig. 7. Instability for all wavelengths for $p_m = 0.65$ and $\eta_m = 2.5632$.

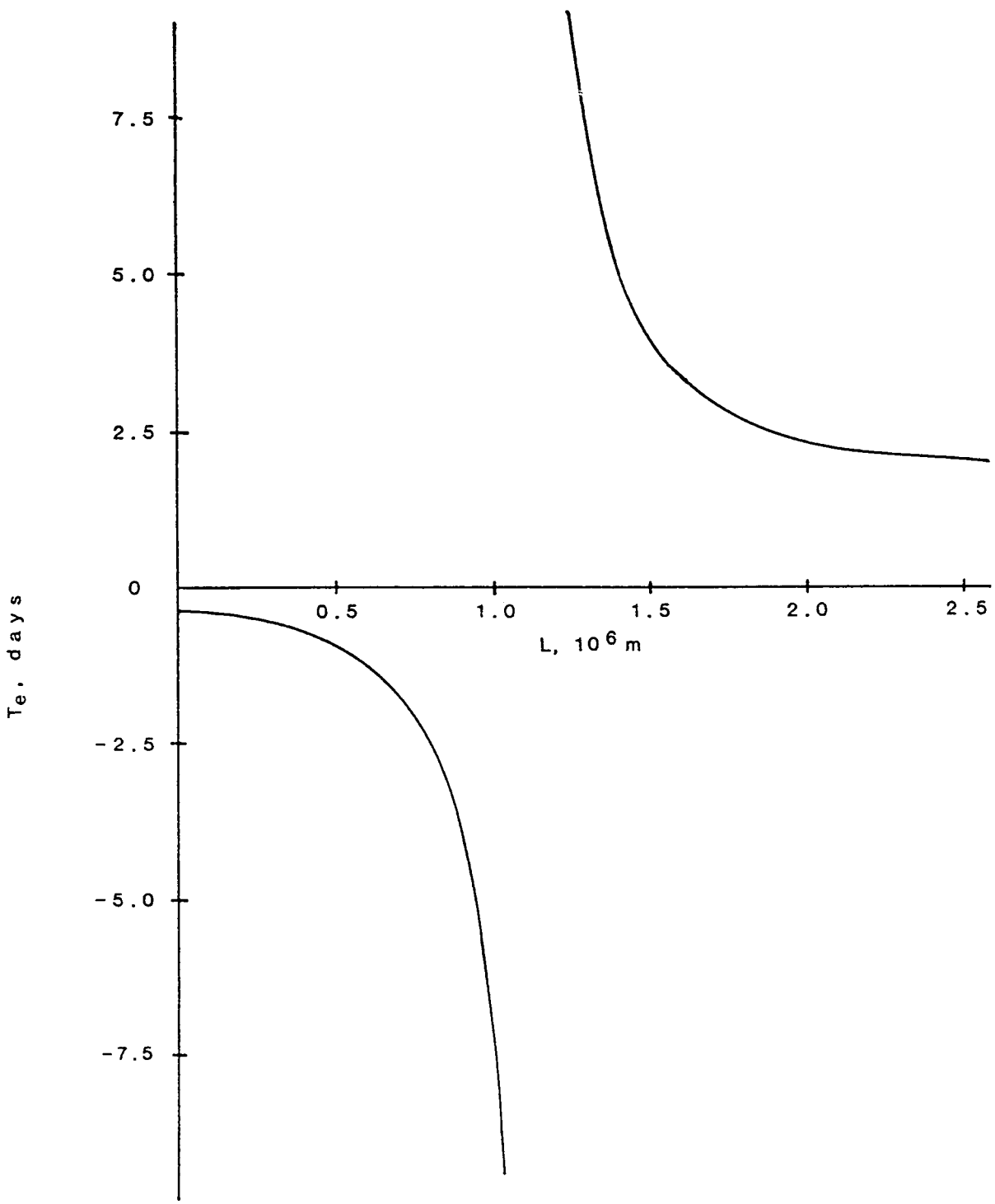

Fig. 8. For $p_m = 0.90$ one finds $\eta_m = -0.7922$ and thus a maximum in the upper atmosphere. It results in stability for short waves and instability for long waves (compare Fig. 5).

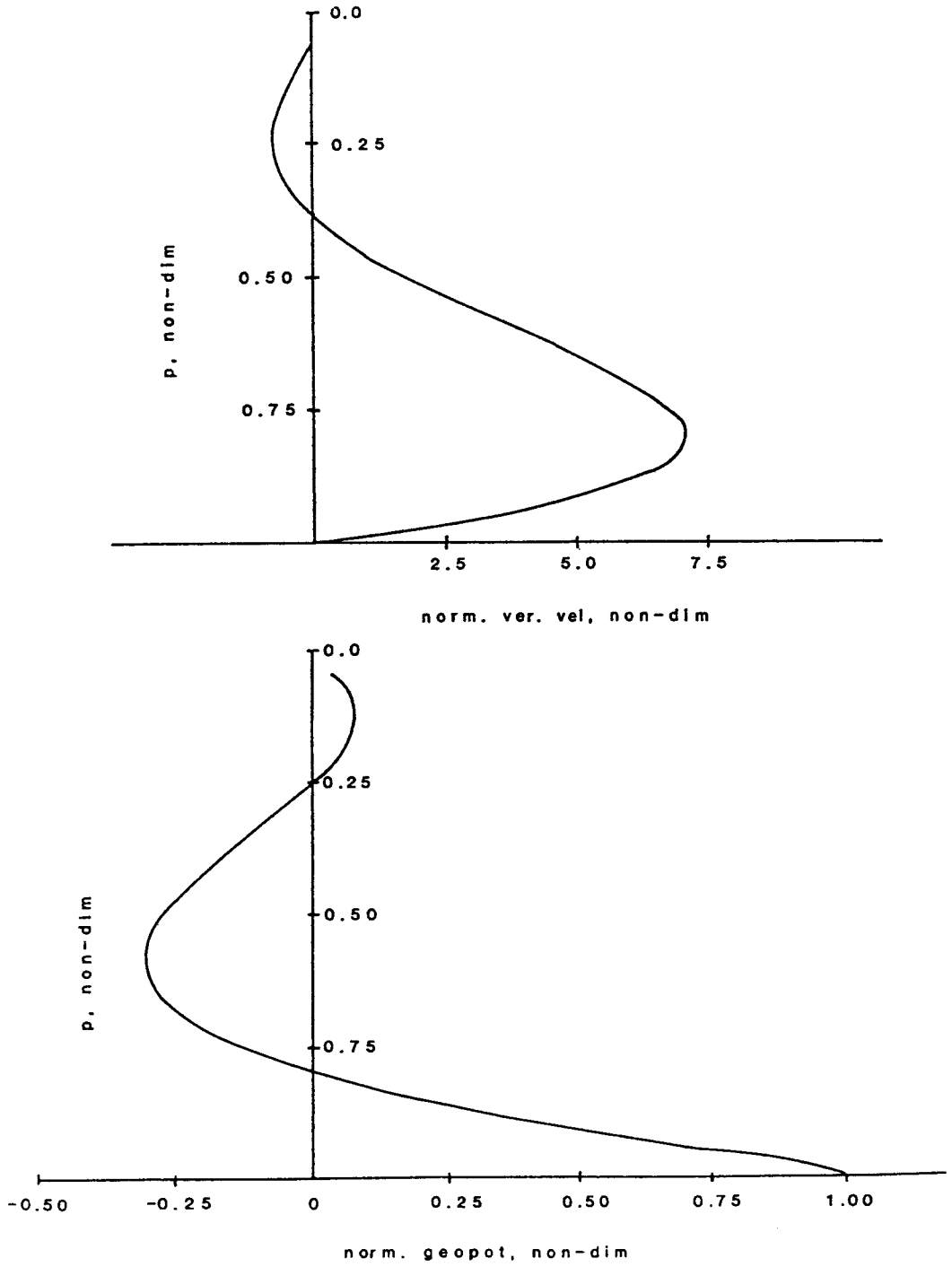

Fig. 9. The non-dimensional vertical velocity and the geopotential for $p_m = 0.8$ and $L = 100$ km.

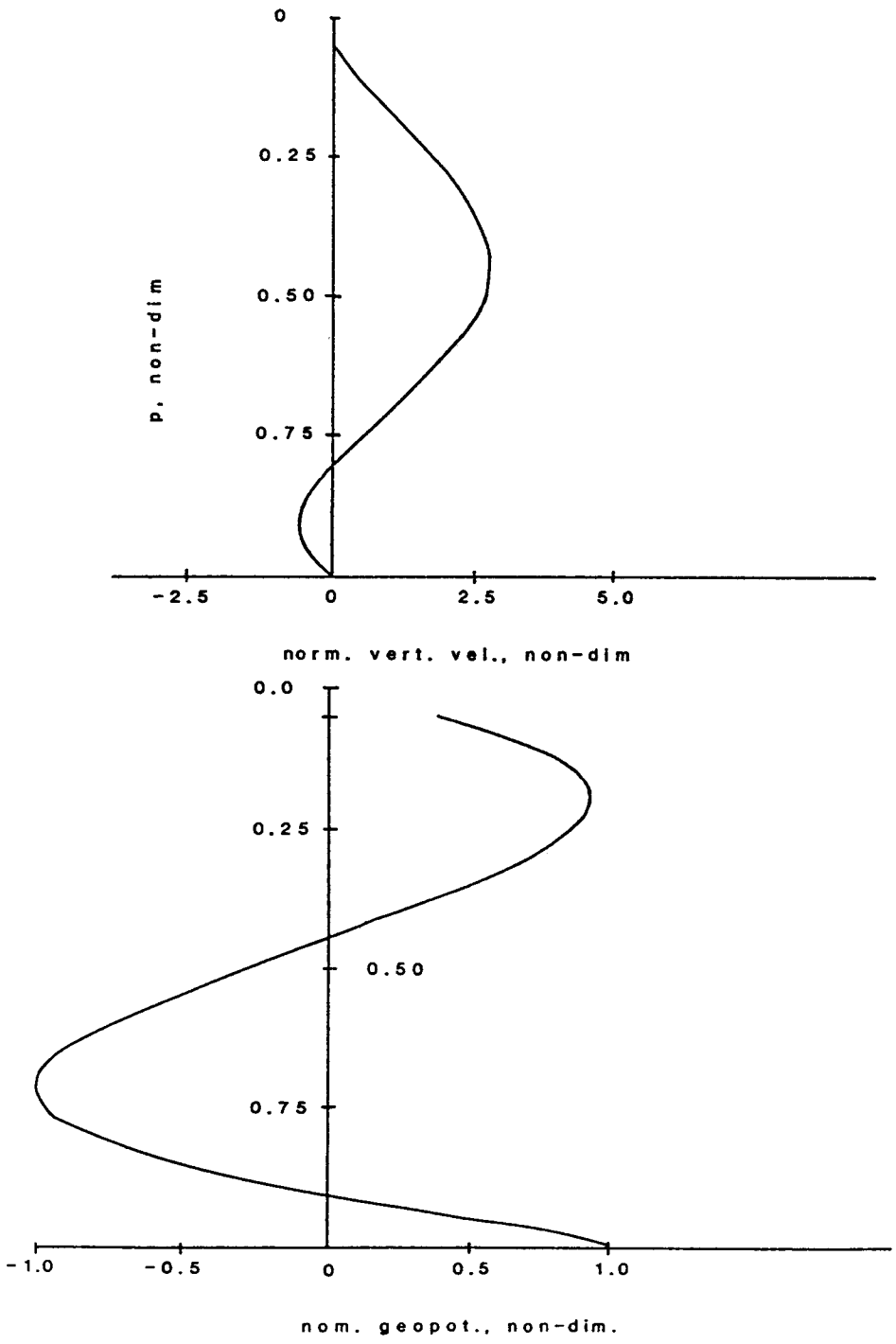

Fig. 10. As Fig. 9, but for $p_m = 0.45$ and $L = 100$ km, representing a stable case.

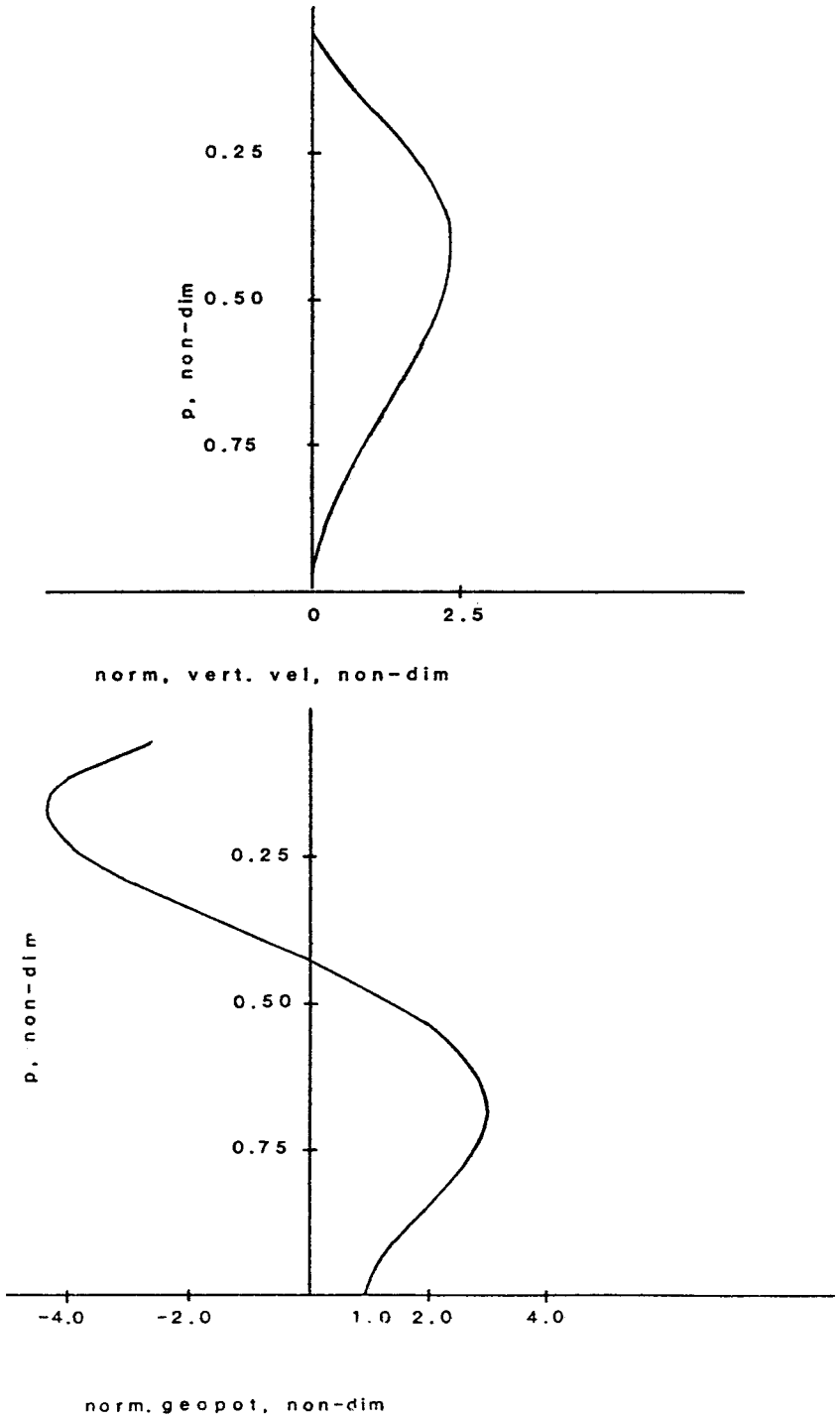

Fig. 11. The case of $p_m = 0.45$ and $L = 1500$ km representing a case of instability.

4. The case of the primitive equations

A number of conditions has to be fulfilled to apply quasi-geostrophic theory to atmospheric problems (Phillips, 1963). Strictly speaking these requirements are not satisfied for the cases treated in Sections 2 and 3 because the important scale in the CISK-problem is too small. Another condition is that the intensity of the heating should not be too large. Phillips (*loc.cit.*) estimated that the heating should be less than 0.1 kJt^{-1} s^{-1}. Using (2.13) and (2.5) we find that:

$$H = Lq\frac{\epsilon}{f_o}\zeta_o \tag{4.1}$$

calculated per unit mass and per unit time. Employing the values quoted in section 2 and $\zeta_o = 10^{-5}$ s^{-1} we find:

$$H = 1.6 \times 10^{-2} kJt^{-1}s^{-1} \tag{4.2}$$

which is about an order of magnitude less than the estimated upper limit, but we should remember that the value used for the relative vorticity is rather small. However, it appears that the condition for the heating intensity could be satisfied.

We formulate a more general system consisting of the vorticity, the divergence, the continuity and the thermodynamic equations. Retaining a basic state of rest and assuming that the vertical distribution of the static stability obeys (2.1) we introduce the same non-dimensional pressure and disregard the beta-effect. Denoting the streamfunction by ψ, the velocity potential by χ and otherwise using the same notations and formulations as before we get the following system:

$$\frac{\partial \nabla^2 \Psi}{\partial t} = \frac{f_o}{p_o}\frac{\partial \omega}{\partial p} \tag{4.3}$$

$$\frac{\partial \nabla^2 \chi}{\partial t} = -\nabla^2 \phi + f_o \nabla^2 \Psi$$

$$p_o \nabla^2 \chi + \frac{\partial \omega}{\partial p} = 0$$

$$\frac{\partial}{\partial t}\left(\frac{\partial \phi}{\partial p}\right) + p_o \sigma \omega = p_o \sigma \omega_B \eta(p)$$

Using the same perturbations as before we get:

$$-k^2 \nu \Psi = \frac{f_o}{p_o}\frac{d\omega}{dp} \tag{4.4}$$

$$-\nu\chi = \phi - f_o\Psi$$

$$-p_o k^2 \chi + \frac{d\omega}{dp} = 0$$

$$\nu\frac{d\phi}{dp} + p_o\sigma\omega = p_o\sigma\omega_B\eta(p)$$

The next step is the process of elimination with the purpose of obtaining a single equation containing the geopotential only. We begin by solving the first equation in (4.4) for ψ and the third for χ. The result is inserted in the second equation with the result that

$$\frac{d\omega}{dp} = -\frac{\nu p_o k^2}{f_o^2(1+\nu^2/f_o^2)}\phi \tag{4.5}$$

For ω_B we use the previous result that:

$$\omega_B = -\frac{gk_F}{f_o}\zeta_o = \frac{gk_F k^2}{f_o}\Psi_o \tag{4.6}$$

Using the first equation in (4.4) combined with (4.5) we find:

$$\Psi = \frac{1}{f_o(1+\nu^2/f_o^2)}\phi \tag{4.7}$$

The last step is to insert (4.5) and (4.7) in the last equation in (4.4) after it has been differentiated with respect to p. The result is:

$$\nu\left[\frac{q^2}{k^2}\lambda(n)^2 + \frac{1}{1+\nu^2/f_o^2}\right]\phi(n) + \frac{\epsilon h(n)}{1+\nu^2/f_o^2}\sum_{s=1}^{n}\phi(s)G_s(1) = 0 \tag{4.8}$$

in which we have introduced the vertical structure functions employed in section 2. The following notations have been introduced:

$$\lambda(n)^2 = 1/4 + \mu(n)^2 \tag{4.9}$$

$$\mu(n)^2 = \frac{n^2\pi^2}{\xi_T^2};\ \xi_T = -1n(p_T)$$

$$\epsilon = \frac{gk_F}{p_o} = 2.2\times 10^{-6}s^{-1}$$

We recall from the previous sections that

$$\hat{\phi}(p) = \sum_{n=1}^{N}\Phi(n)G_n(p) \tag{4.10}$$

$$\hat{\phi}_o = \sum_{n=1}^{N}\Phi(n)G_n(1)$$

$$h(p) = \frac{d\eta}{dp} = \sum_{n=1}^{N}h(p)G_n(p)$$

One of the conditions for the application of quasi-geostrophic theory is that $\nu << f_o$. If this

were the case (4.8) would reduce to the problem solved in section 2. The determination of ν from (4.8) is a non-standard eigenvalue problem. However, for a given choice of the total number of components N, (4.8) is still a homogeneous set of linear equations in the amplitudes $\Phi(n)$. The condition for a non-trivial solution is thus that the determinant vanishes. This procedure leads to an algebraic equation for ν, but if N is large we get an equation of a high degree.

To evaluate the determinant for the system (4.8) we proceed in a way which is analogous to the method used in section 2. We introduce the notations:

$$r(n) = \frac{q^2}{k^2}\lambda(n)^2; \; z = \frac{\nu}{f_o} \tag{4.11}$$

and start by eliminating all variables except $\Phi(1)$ and $\Phi(2)$ from the first two equations by multiplying the first by $h(2)$ and the second by $h(1)$ followed by subtraction. The result is:

$$\frac{\Phi(1)}{\Phi(2)} = \frac{1+r(2)(1+z^2)}{1+r(1)(1+z^2)}\frac{h(1)}{h(2)} \tag{4.12}$$

An analogous procedure is the used on the second and the third equation, the third and the fourth, and finally on the equations with the numbers $(N-1)$ and N. All the relations corresponding to (4.12) can be written as a general expression:

$$\frac{\Phi(n)}{\Phi(N)} = \frac{1+r(N)(1+z^2)}{1+r(n)(1+z^2)}\frac{h(n)}{h(N)} \tag{4.13}$$

These relations are entered in the N'th equation which then contains the common factor $\Phi(N)$. Its coefficient must then vanish with the result that:

$$z + \sum_{n=1}^{N} \frac{(\epsilon/f_o)G_n(1)h(n)}{1+r(n)(1+z^2)} = 0 \tag{4.14}$$

From (4.14) it is seen that a truncation at N leads to an algebraic equation of degree $(2N+1)$. As a first case we use $N = 2$. Written out as a 5'th degree equation (4.14) becomes:

$$\sum_{r=0}^{5} a_r z^r = 0 \tag{4.15}$$

where

$$a_5 = r(1)r(2) \tag{4.16}$$

$$a(4) = 0$$

$$a_3 = r(1) + r(2) + 2r(1)r(2)$$

$$a_2 = \frac{\epsilon}{f_o}[h(1)G_1(1)r(2) + h(2)G_2(1)r(1)]$$

$$a_1 = 1 + r(1) + r(2) + r(1)r(2)$$

$$a_o = \frac{\epsilon}{f_o}[h(1)G_1(1) + h(2)G_2(1)] + a_2$$

The roots in (4.15) may be classified as four roots of the gravity-inertial type and one root corresponding to the quasi-geostrophic mode. The former roots are obtained in a pure form if $h(1) = h(2) = 0$. Solving (4.15) in this case of no heating we find four purely imaginary roots meaning that the waves are neutral waves. The non-dimensional frequency is:

$$z = \pm i(1 + \frac{k^2}{q^2\lambda(n)^2})^{1/2};\ n = 1,\ 2 \tag{4.17}$$

We recall that $h(1)$ and $h(2)$ cannot be given arbitrary values since the integral conditions (2.15) has to be fulfilled. For $h(n)$ we have:

$$\frac{d\eta}{dp} = \sum_{n=1}^{N} h(n)G_n(p) \tag{4.18}$$

Integrating and setting $\eta(1) = 0$ we find:

$$\eta(p) = \sum_{n=1}^{N} 2D(n)h(n)\exp(-1/2\xi)\sin(\mu(n)\xi) \tag{4.19}$$

where $D(n)$ is the normalization factor given by Wiin-Nielsen and Marshall (1990) and $\xi = -\ln(p)$. In our case of just two components we find when (4.19) is inserted in (2.15) that:

$$\frac{8D(1)\mu(1)}{1+4\mu(1)^2}(1 + \exp(-1/2\xi_T)h(1)) + \frac{8D(2)\mu(2)}{1+4\mu(2)^2}$$

$$(1 - \exp(-1/2\xi_T)h(2)) = E_o \tag{4.20}$$

We know that $(d\eta/dp)_1$ is an important factor in the determination of the stability, because also in this generalized case we find for $L = 0(k \to \infty)$ that:

$$z = -\frac{\epsilon}{f_o}\sum_{n=1}^{N} G_n(1)h(n) \tag{4.21}$$

This is true because for $k \to \infty$ we find $r(n) = 0$ for all n, and (4.21) follows then from (4.14). If we want to control the stability for $L = 0$ it is then convenient to write:

$$G_1(1)h(1) + G_2(1)h(2) = \left(\frac{d\eta}{dp}\right)_1 \tag{4.22}$$

We start by considering a moderate 2-component case with $h(1) = 2$ and $h(2) = 10.4277$ satisfying (4.20). Equation (4.15) was solved for $0 < L < 2500$ km. For each value of the wavelength we found one real, positive root indicating instability and four complex roots which have a negative real part indicating damping. The positive real root for z is in each case compared with the solution for z in the quasi-geostrophic case. The two roots are almost equal with a difference which is at most 0.64% of the value for the primitive equations. The values of z ranges from 0.13 to 0.21, and our results indicate therefore agreement with the fact that quasi-geostrophic theory is applicable when the frequency is much smaller than the Coriolis parameter. The values of z as a function of the wavelength are shown in Figure 12. The values for the gravity-inertial waves were also compared with values computed from (4.17) with the result that corresponding values differ by less than 1%. These results are due to the fact that the derivative of η for $p = 1$ is small in this case.

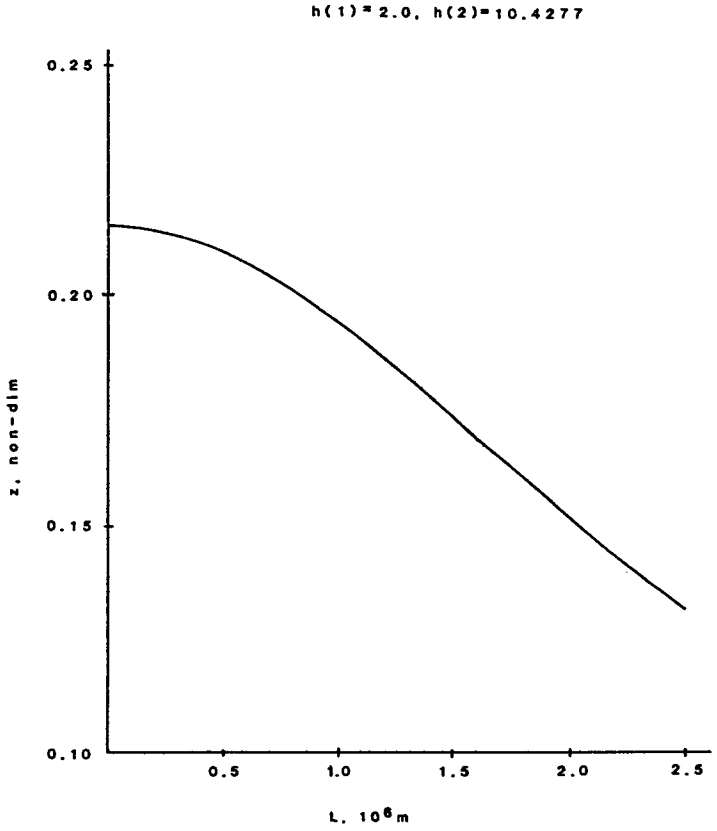

Fig. 12. The non-dimensional frequency as a function of wavelength for the primitive equations with just two vertical structure functions.

These results are not generally true because we may construct other cases where $\nu/f_o > 1$. As a second example we select $h(1) = -27.86$ and $h(2) = 152.69$. It was designed in such a way that it has about the same value for $(d\eta/dp)_1$ as the example defined used in section 3.

Figure 13 shows ν/f_o as a function of the wavelength for the two models. We find that the frequency is larger than the Coriolis parameter for $0 < L < 2000$ km. The differences are now large as could be expected. For $L = 0$ there is no difference, but for $L = 1000$ km the difference is 29% and for $L = 2000$ km it is 40%.

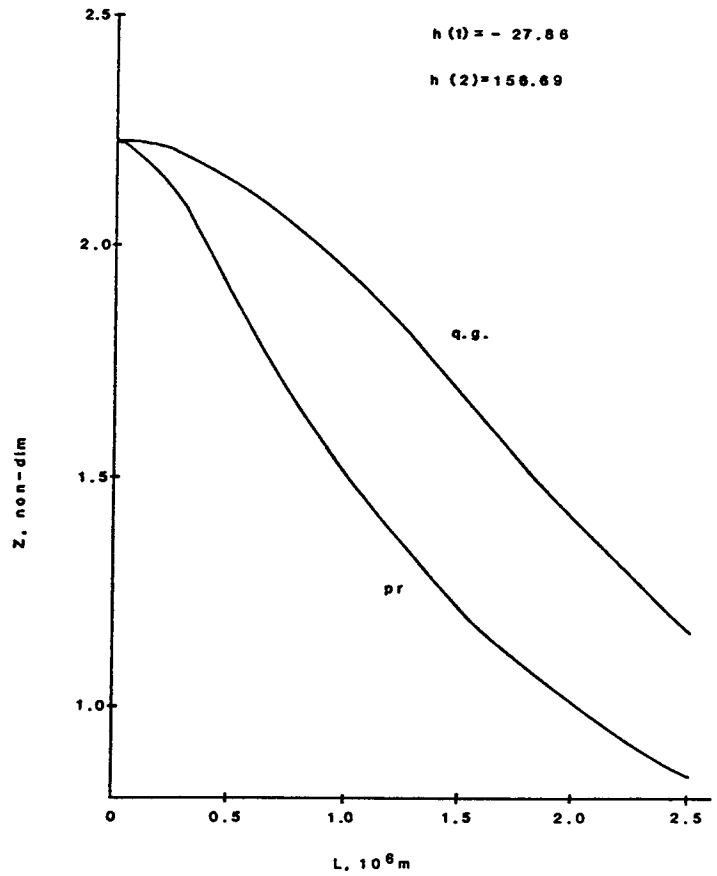

Fig. 13. The non-dimensional frequencies as a function of wavelength for the primitive equations and the quasi-geostrophic equations with two vertical structure functions.

A comparison between the non-dimensional frequencies for the gravity-inertial modes in the two cases indicate that the imaginary part, related to the wave speed, changes very little (see Fig. 14). Changes are, however, found in the real parts. As mentioned in the discussion of the first case the gravity-inertial waves were stable for all wavelengths in that case. This is not so in the second example. However, the real part of the frequency for the gravity-inertial modes is much smaller than the frequency for the meteorological model (compare Fig. 13 and Fig. 15).

We conclude therefore that the 2-component cases discussed here seem to indicate that the primitive equations should be used whenever the heating gradient at the surface becomes so large that $z > 1$.

During the present study it has become clear that the formulation of vertical velocity at the top of the boundary layer, which depends on the surface vorticity, should be expressed in terms of the streamfunction. It is naturally tempting to use a geostrophic approximation in terms of the geopotential because it makes the elimination procedure much simpler. However, if this is done, it can be demonstrated that a false eigenvalue is introduced. This particular eigenvalue represents an unstable solution with a small e-folding time, and it will thus dominate a numerical integration. The detailed demonstration of the above statement is not reproduced here, but it can for example be shown that it is the case if one takes the special case of $L = 0$. In addition, numerical integrations carried out by Strunge Pedersen (*personal communication*) have verified the statements given above.

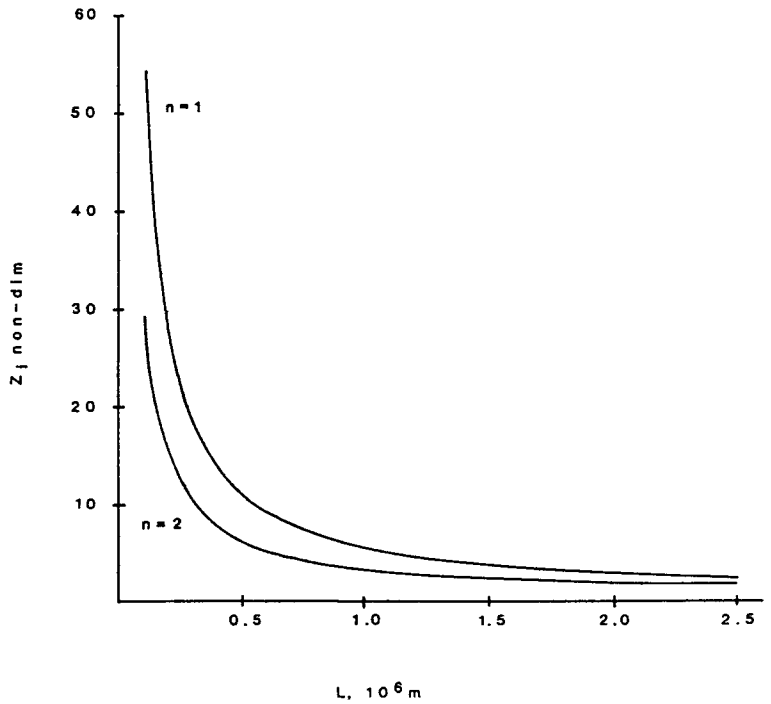

Fig. 14. The imaginary parts of the two frequencies for gravity-inertial waves as a function of wavelength.

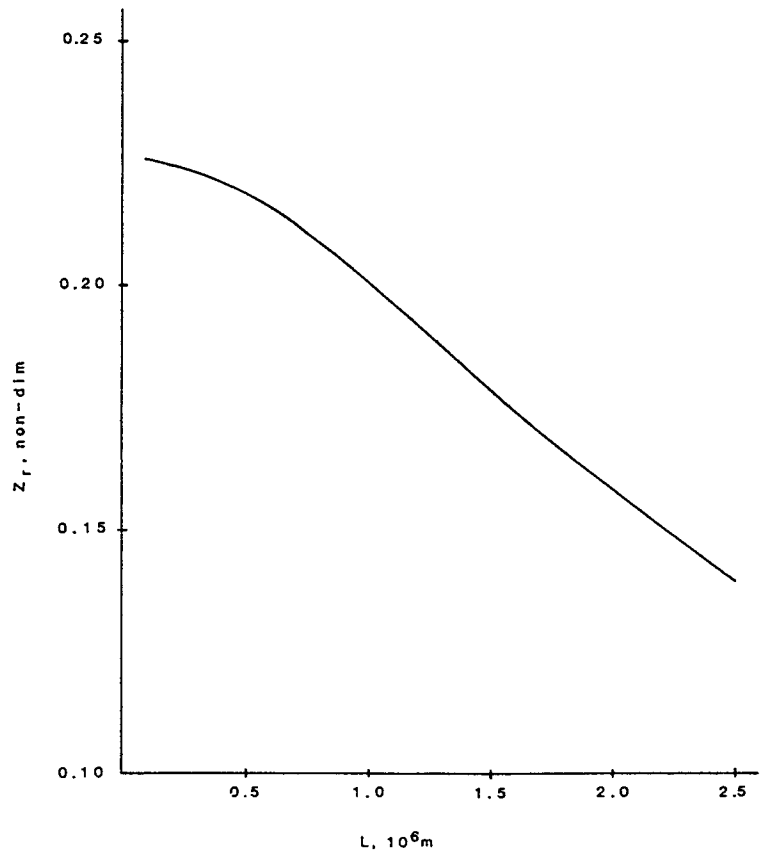

Fig. 15. The real part of the frequency for gravity-inertial waves as a function of wavelength.

Considering the general equation (4.14) it is to be expected that the $2N+1$ roots will represent N pairs of quasi-inertial modes and one mode corresponding to quasi-geostrophic motion. If we limit the interest to the single real root in the equation, it is much easier to solve the problem by numerical procedures. This has been done for the heating profile used in section 3. Figure 16 shows for $p_m = 0.8$ the e-folding times for the quasi-geostrophic case and the case of the primitive equations. The two solutions coincide for $L = 0$ as they should. Otherwise the primitive equations result in somewhat larger e-folding times than the quasi-geostrophic equations. The difference is largest for the intermediate waves, and it amounts to about 15% where it is largest.

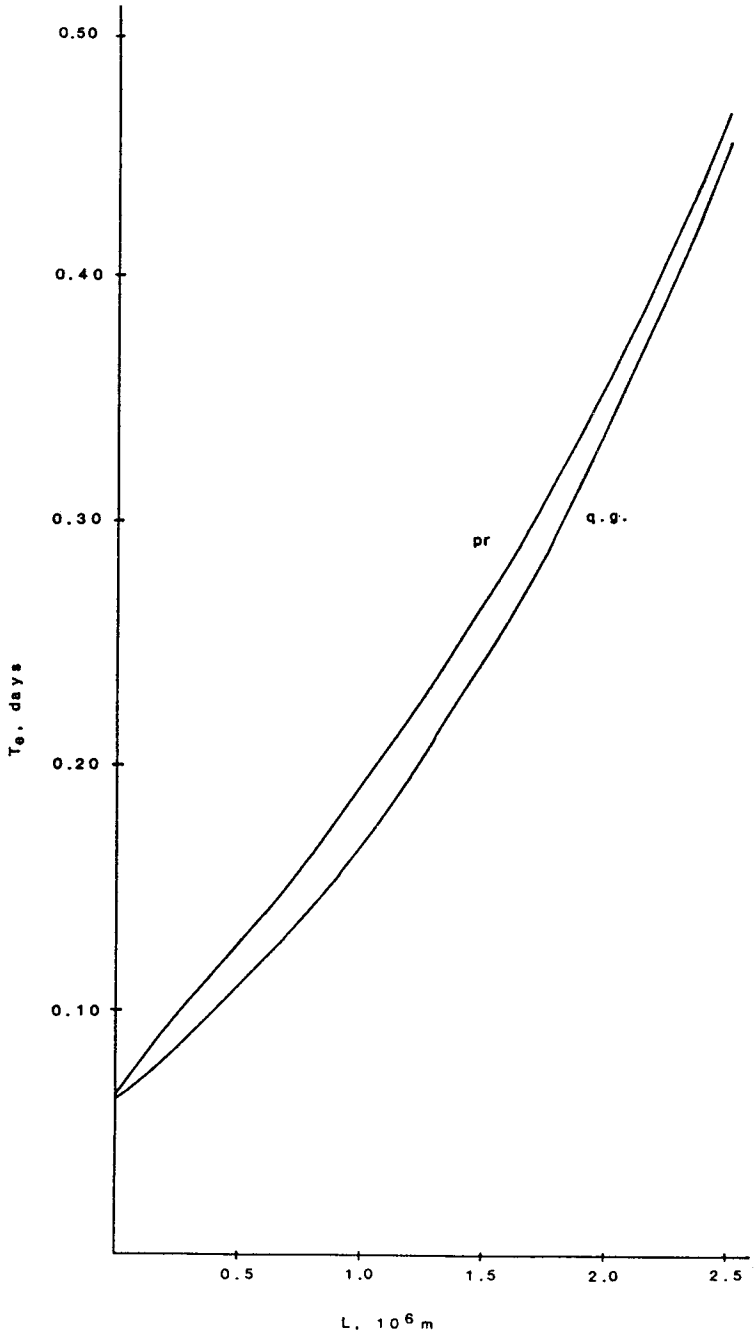

Fig. 16. The e-folding times for the primitive and the quasi-geostrophic cases as a function of wavelength where the number of structure functions is $N = 100$.

Having solved the eigenvalue problem for this single mode we may proceed to look at its structure. From the basic equations it is seen that:

$$\hat{\chi}(p) = -z\hat{\Psi}(p) \tag{4.23}$$

$$\hat{\Psi}(p) = \frac{1}{1+z^2}\frac{1}{f_o}\hat{\phi}(p)$$

$$\hat{\chi}(p) = \frac{z}{1+z^2}\frac{1}{f_o}\hat{\phi}(p)$$

While Figure 16 shows that the difference in growth rate may be moderately large, we can use (4.23) to show that the difference in other parameters may differ considerably. The first relation in (4.23) gives also the ratio of the divergence to the vorticity, i.e.

$$\nabla \cdot \vec{v}/\zeta = -z \tag{4.24}$$

which is shown in Figure 17. The minus-sign indicates as expected that the divergence and the vorticity have opposite signs, i.e., convergence connected with cyclonic vorticity and vice versa.

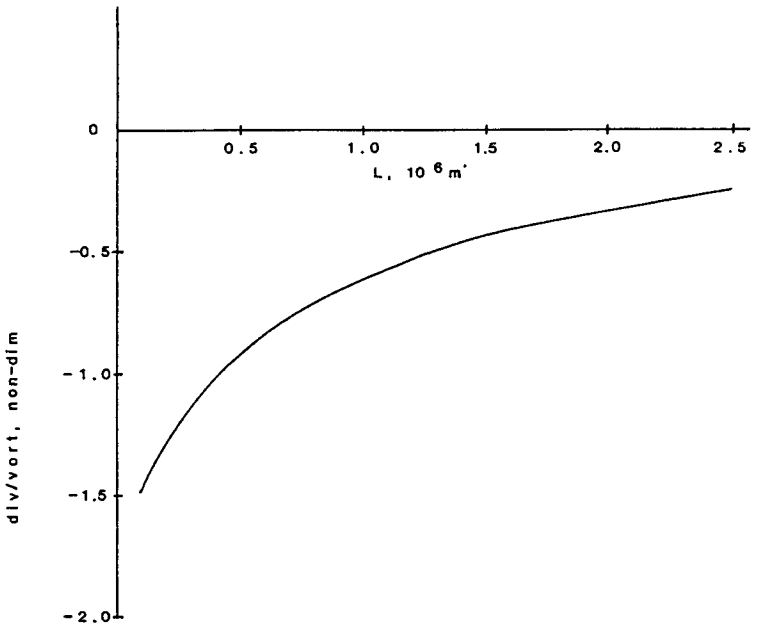

Fig. 17. The ratio of divergence and vorticity as a function of wavelength using the case of Fig. 16.

For very small wavelengths the divergence is larger than the vorticity, while the numerical value decreases to a ratio of 1/4 for the longest waves included in the investigation. The second relation in (4.23) can be used to express the ratio of the meridional component of the wind and the geostrophic wind component in the same direction. this ratio is:

$$\frac{v}{v_g} = \frac{1}{1+z^2} \tag{4.25}$$

and it is shown in Figure 18. Strong a-geostrophic components exist for the short waves, but the ratio comes closer to unity as the wavelength increases.

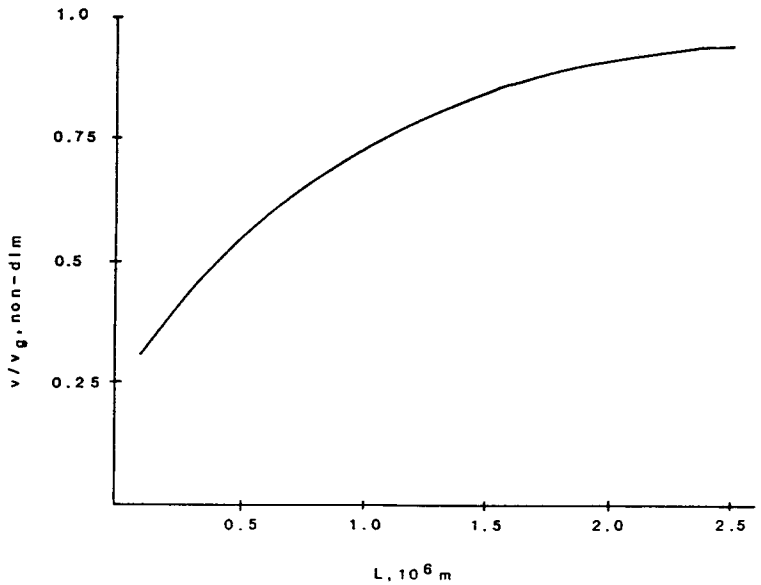

Fig. 18. The ratio of the meridional wind component and the geostrophic value of the same component as a function of wavelength using the case of Fig. 16.

The main conclusion is thus that for the example chosen here, where the maximum in the heating distribution is relatively close to the surface of the Earth, we need the primitive equations to give a correct distribution. On the other hand, if the maximum were at a higher level giving a small, but positive value of z, the situation is much closer to the quasi-geostrophic case. As an example we may mention that if the maximum heating is at $p_m = 0.55$ then z varies between 0.10 and 0.15, the ratio of the divergence to the vorticity varies from -0.15 to -0.10, and the ratio of the two wind components is always above 0.98. With respect to the vertical changes it follows from (4.23) that:

$$\frac{\hat{\phi}(p)}{\hat{\phi}(1)} = \frac{\hat{\Psi}(p)}{\hat{\Psi}(1)} = \frac{\hat{\chi}(p)}{\hat{\chi}(1)} \tag{4.26}$$

It is thus sufficient to calculate only one of the parameters and the surface values of the other.

5. Summary and conclusions

The study contains a number of solutions of increasing generality of the CISK problem. The quasi-geostrophic problem is solved for a continuous vertical variation of the dependent variables and for a static stability, which varies inversely proportional to the square of the pressure. Exact solutions can be obtained, but they contain power functions where the exponent becomes extremely large for small values of the wavelength preventing any accurate calculation. Since the smaller horizontal scales are of particular interest in the CISK problem, it becomes desirable to formulate the problem in a different way which will permit more accurate determinations of the results.

Vertical structure functions are employed for this purpose. The dependent variables are expressed as sums of products of coefficients, depending generally on the horizontal coordinates and time, and the structure functions which form a set of normalized, orthogonal functions. Such a procedure is not ideal either because the upper boundary condition has to be applied

at a pressure which is different from zero. The two solutions are compared with the result that they are identical for all practical purposes for the wavelengths for which the exact solution can be computed with accuracy. It is also shown that the two solutions have the same value for the special case of a vanishing wavelength.

As one would expect, the method requires a large number of structure functions to give convergence and good accuracy. However, the numerical difficulties have disappeared except for extremely small scales.

To illustrate the procedure a flexible heating distribution function was designed, permitting a selection of the pressure at which an extremum will occur.

The main results of the investigation are that instability will exist for all wavelengths if the heating maximum is located in the lower part of the troposphere, but not very close to the surface. A maximum in the upper part of the troposphere will on the other hand lead to stability for all wavelengths. Heating maxima at intermediate levels will result in instability for small values of the wavelength and stability for large values of the same parameter.

A treatment is given of the behavior of the CISK mechanisms in a linearized primitive equations model. It leads to a non-standard eigenvalue problem which may be solved by finding all (complex) roots to a high degree polynomial. Using first a model with only two vertical structure functions it is found that the primitive equations lead to solutions which are less unstable than the corresponding solutions in the quasi-geostrophic case. It is also found that the 5 solutions consist of 2 pairs of gravity-inertial waves and a single mode corresponding to a meteorological wave. The model is also used to verify that the position of the heating maximum also in this case is very important for the instability of the waves.

For the general case it is realized that the $(2N + 1)$ solutions will be pairs of quasi-inertial waves and a single meteorological mode. The latter mode is characterized by having a real frequency which may be positive or negative. In view of this distribution it was decided to concentrate on the real roots in the general equation. It was verified that only one such solution exists. A comparison between the solutions of the primitive equations and the quasi-geostrophic equations confirm the earlier result that the primitive equations result in less unstable solutions. The largest difference is found to occur for the waves of intermediate wavelength in the interval 0 to 2000 km.

A comparison is made between the vertical structures of the two solutions to investigate how non-geostrophic the solutions from the primitive equations are. This is done by computing the ratio of the divergence and the vorticity and the ratio of the meridional wind component and the corresponding geostrophic value. The most non-geostrophic waves are those of small wavelength.

It is finally mentioned that the surface vorticity entering the expression for the vertical velocity at the top of the boundary layer should be expressed consistently by the Laplacian of the streamfunction and not by using a geostrophic assumption. The latter procedure will result in a false unstable solution.

6. Acknowledgements

The author expresses his gratitude to T. Strunge Pedersen for many discussions of the problems treated in this paper, and his appreciation to Ms. Conny Jensen who has prepared the figures for the paper. The constructive remarks by two referees have hopefully resulted in an improved paper.

REFERENCES

Charney, J. G. and A. Eliassen, 1964. On the growth of the hurricane depression, *J. Atmos. Sci.*, **21**, 68-75.

Christensen, C. and A. Wiin-Nielsen, 1991. A study of global mean temperatures applied to available potential energy, annual variations and static stability, *Tellus*, **43A**,15-24.

Fräedrich, K. and J. L. McBride, 1989. The physical mechanism of CISK, and the free ride balance, *J. Atmos. Sci.*, **46**, 2642-2648.

Kasahara, A. and H. L. Tanaka, 1989. Application of vertical normal mode expansion to problems of baroclinic instability, *J. Atmos. Sci.*, **46**, 489-510.

Ooyama, K., 1964. A dynamical model for the study of tropical cyclone development, *Geofís. Int.*, **4**, 187-198.

Pedersen, T. S., 1991. A comparison of the Free Ride and CISK assumptions, *J. Atmos. Sci.*, **48**, 1813-1821.

Phillips, N. A., 1963. Geostrophic motion, *Rev. Geophys.*, **1**, No. 2, 123-176.

Rasmussen, E. A., 1979. The polar low as an extratropical CISK disturbance, *Quart. J. Roy. Met. Soc.*, **105**, 531-549.

Wiin-Nielsen, A. and H. Marshall, 1989. On the relative structure of transient atmospheric waves, *Vejrt, Danish Met. Soc.* (Special issue in English), 49-64.

Wiin-Nielsen, A. and H. Marshall, 1990. Part III, On the structure of transient atmospheric waves, *Atmósfera*, **3**, 73-109.